Backbone Dynamics of TEM-1 Determined by NMR: Evidence for a Highly Ordered Protein†

Pierre-Yves Savard and Stéphane M. Gagné*

Département de Biochimie et de Microbiologie and CREFSIP, Université Laval, Québec, Canada G1K 7P4

Received March 2, 2006; Revised Manuscript Received June 5, 2006

ABSTRACT: Backbone dynamics of TEM-1 β-lactamase (263 amino acids, 28.9 kDa) were studied by ^{15}N nuclear magnetic resonance relaxation at 11.7, 14.1, and 18.8 T. The high quality of the spectra allowed us to measure the longitudinal relaxation rate (R_1), the transverse relaxation rate (R_2), and the $\{^1H\}-^{15}N$ NOE for up to 227 of the 250 potentially observable backbone amide groups. The model-free formalism was used to determine internal motional parameters using an axially anisotropic model. TEM-1 exhibits a small prolate axial anisotropy ($D_\parallel/D_\perp = 1.23 \pm 0.01$) and a global correlation time (τ_m) of 12.41 ± 0.01 ns. The unusually high average generalized order parameter (S^2) of 0.90 ± 0.02 indicates that TEM-1 is one of the most ordered proteins studied by liquid-state NMR to date. Although the Ω-loop has a high degree of order in the picosecond-to-nanosecond time scale (mean S^2 value of 0.90 ± 0.02), we observed the presence of microsecond-to-millisecond time scale motions for this loop, as for the vicinity of the active site. These motions could be relevant for the catalytic function of TEM-1. Amide exchange experiments were also performed, and several amide groups were not exchanged after 12 days, an indication that global motions in TEM-1 are also very limited. Although detailed dynamics characterization by NMR cannot be readily applied to TEM-1 in the presence of relevant substrates, the unusual picosecond-to-nanosecond dynamics behavior of TEM-1 presented here will be essential to the validation and improvement of future molecular dynamics simulations of TEM-1 in the presence of functionally relevant substrates.

It has long been known that antimicrobial resistance is a growing public health problem (*1*). Tuberculosis, gonorrhea, malaria, and childhood ear infections are just a few of the diseases that have become hard to treat with antibiotic drugs, and ∼70% of bacteria that cause infections in hospitals are resistant to at least one of the drugs most commonly used (http://www.fda.gov/oc/opacom/hottopics/anti_resist.html). β-Lactam antibiotics, such as penicillins, were discovered by Fleming 75 years ago and were targeted immediately by highly adaptable bacteria. β-Lactam antibiotics inhibit the DD-peptidases (members of the penicillin binding proteins family) which are responsible for the construction of the peptidoglycan, a major constituent of the bacterial cell wall. β-Lactamases are the most prevalent weapons developed by bacteria to fight against these antibiotics. These enzymes are very efficient at hydrolyzing irreversibly the β-lactam ring of β-lactam antibiotics by an acylation−deacylation mechanism. β-Lactamases are often classified in four classes based on their amino acids sequences (*2*). Classes A, C, and D include active serine enzymes, while class B consists of metalloenzymes. Among the class A enzymes, TEM-1 (263 residues, 28.9 kDa) is by far the most studied by several techniques such as X-ray crystallography (*3*−*5*), molecular dynamics (MD)[1] simulations (*6*−*9*), electron−nuclear double-resonance spectroscopy (ENDOR) (*10*, *11*), and NMR (*12*−*14*). Despite all of these studies, aspects of the mechanism of action of catalytic residues in this protein still remain unclear and controversial. To date, there are more than 100 naturally occurring mutants of TEM (http://www.lahey.org/Studies/temtable.asp); the list is growing along with the development of new antibiotics, so there is an urgent need to better understand this mechanism of action.

According to previous studies, the most important residues for catalysis in TEM-1 are Ser70 (catalytic serine), Lys73, Ser130, Glu166, and Lys234. There is a general consensus about the deacylation part of the mechanism, which would be performed by the carboxylate of Glu166 which activates a water molecule that hydrolyzes the ester bond of the acyl−enzyme intermediate (*3*, *15*, *16*). The acylation part is, however, not as clear and somewhat controversial. Several hypotheses about the TEM-1 acylation mechanism are found in the literature, and only some of them will be presented here. One of these hypotheses implies that Glu166 acts as the general base by abstracting the proton of Ser70. As Glu166 and Ser70 seem to be too far away to interact directly, it was proposed that this mechanism would proceed either via a water molecule (*5*, *17*) or by a certain mobility

† This work was supported by the NSERC (Grant 250084), and equipment was purchased with funding from CFI and MEQ (Grant 7250).

* To whom correspondence should be addressed: 3255 pavillon Marchand, Université Laval, Québec, QC, Canada G1K 7P4. Phone: (418) 656-7860. Fax: (418) 656-7176. E-mail: sgagne@rsvs.ulaval.ca.

[1] Abbreviations: NMR, nuclear magnetic resonance; NOE, nuclear Overhauser effect; MD, molecular dynamics; ENDOR, electron−nuclear double-resonance spectroscopy; QM/MM, quantum mechanical and molecular mechanical; IPTG, isopropyl β-D-thiogalactoside; SDS−PAGE, sodium dodecyl sulfate−polyacrylamide gel electrophoresis; LC−MS, liquid chromatography−mass spectrometry; HSQC, heteronuclear single-quantum coherence; DSS, sodium 2,2-dimethyl-2-silapentane-5-sulfonate; CD, circular dichroism.

10.1021/bi060414q CCC: $33.50
Published on Web 08/31/2006

of the Ω-loop in solution to allow the distance between these residues to be shortened during the acylation process (*9*, *18*). In another hypothesis, Lys73 acts as the general base in the acylation by abstracting the proton of Ser70 and transferring it to the nitrogen of the β-lactam ring (*3*, *19*). In this latter suggestion, Lys73 should be deprotonated and, thus, have a pK_a of <10.0.

Recent studies have produced favorable evidence for both mechanisms. From an ultra-high-resolution X-ray structure of TEM-1 (0.85 Å), Minasov et al. (*5*) suggest a symmetric mechanism in which Glu166 is the catalytic base activating Ser70 via a water molecule. Their conclusions are based on the observation of a protonated Glu166 at pH 8.0 and on its participation in a hydrogen-bonding network that extends to the nucleophilic serine. They also propose that the leaving group lactam nitrogen would be activated by accepting a proton from Ser130. Lys73 would be responsible either for the electrostatic activation of Ser70 and Ser130 or for the proton transfer to Ser130. The authors do not, however, exclude the possibility that Lys73 could also be the catalytic base. A similar conclusion was reached from a 1.5 ns MD study (*8*), where Glu166 is identified as the catalytic base acting via the water molecule, with a parallel protonation of the β-lactam ring via a H-bond network involving Glu166, Lys73, a second water molecule, and Ser130. In this latter work, pK_a values measured from the simulations for the lysines in the active site were greater than 10. Another 1.2 ns MD study (*6*) proposed a competitive route for the acylation that could proceed either via Glu166 and water or via the hydroxyl group of Ser130 and the substrate carboxylate group. In agreement with this work is another recent 5 ns MD study (*9*), in which an additional flaplike translational motion of the Ω-loop is observed in the equilibrated part of the simulation. A dual participation of Glu166 and Lys73 was recently proposed by the Mobashery group. On the basis of studies of the protonation state of Lys73 (*14*) and ab initio QM/MM calculations (*7*), they conclude that both mechanisms could compete to promote the Ser70 for the acylation step. More detailed information can be found in the review by Fisher et al. (*20*).

Proteins are not static, and conformational changes which cover a wide range of time scales and amplitudes are intimately linked to biological function. Although the quantitative and functional characterization of these motions on a site-specific basis remains a major challenge, several dynamics parameters can be accessed by solution NMR spectroscopy. It can provide detailed information pertaining to the internal dynamics occurring in proteins over a wide range of biologically relevant time scales (typically picoseconds to nanoseconds, microseconds to milliseconds, and seconds to days). Fast dynamics (picoseconds to nanoseconds) in proteins relate to conformational entropy and can have a significant impact on the energetics of ligand binding. Microsecond-to-millisecond time scale motion may have an effect on enzyme catalysis, rate-limiting conformational transitions, and ligand−protein recognition. The second-day time scale is linked to slow processes such as folding and unfolding.

In an attempt to bring new insight to the characterization of TEM-1, we initiated an experimental characterization of its dynamics using NMR. Taken together, data obtained from the complementary techniques cited above will contribute to a better understanding of the relation among structure, dynamics, and function. Although NMR cannot be readily applied to the study of biologically relevant TEM-1 complexes because of the rapid turnover rate, experimental NMR dynamics characterization will be extremely valuable for the validation and improvement of existing and future MD simulations of TEM-1 in the presence of substrates. This paper describes an analysis of TEM-1 backbone dynamics based on ^{15}N relaxation parameter measurements at field strengths of 11.7, 14.1, and 18.8 T (corresponding ^{1}H frequencies of 500, 600, and 800 MHz, respectively). This is the first structure−dynamics study of a class A β-lactamase carried out in solution by NMR. It provides new insights into the behavior of TEM-1 (and possibly other class A β-lactamases) under near-physiological conditions and could eventually help in the understanding of the fine-tuning behind the acylation mechanism of these proteins.

EXPERIMENTAL PROCEDURES

Overexpression and Purification of ^{15}N-Labeled TEM-1. The *bla* gene, encoding the mature TEM-1, was fused to the ompA signal peptide and subcloned into the pET-24a vector as described previously (*21*), and this construction was used for transformation in *Escherichia coli* BL21(DE3). As explained later, the construct that was used corresponds to the E28G mutant of TEM-1. Uniformly ^{15}N-labeled protein samples were prepared by growing cells on a M9 minimal medium (Sigma) containing $^{15}NH_4Cl$ as the sole nitrogen source (Cambridge Isotope Laboratories), 300 mM sorbitol (Sigma), 2.5 mM betain (Sigma), and 30 μg/mL kanamycin (Roche). The TEM-1 protein was expressed by growing the host cells at 37 °C to an OD_{600} of 0.8 followed by induction with 0.4 mM IPTG (Invitrogen) and addition of 15 μg/mL kanamycin for 16−18 h at 25 °C. Cell cultures were centrifuged, and the supernatant was concentrated 5-fold using a stirred cell (Millipore) with an Amicon YM-10 membrane (molecular mass cutoff of 10 000 Da). The concentrate was then loaded on a DEAE-Sepharose Fast Flow anion exchange column (using an AKTA Explorer from GE Healthcare) pre-equilibrated with a 10 mM Bis-Tris propane buffer (pH 6.6) (GE Healthcare), and the protein was eluted with a 0 to 200 mM NaCl linear gradient. No further purification step was necessary, and the resulting protein was very pure as judged by SDS−PAGE and LC−MS. Using this protocol, yields were typically 120 mg of TEM-1/L with 97% ^{15}N incorporation.

NMR Samples. For the collection of NMR spectra, the protein was lyophilized after extensive dialysis against H_2O and was dissolved to a concentration of 0.7 mM in a 25 mM sodium phosphate buffer (pH 6.6), 3.0 mM imidazole as an internal pH reference, a cocktail of protease inhibitors (Roche complete), 0.1% sodium azide, 0.1 mM DSS for internal referencing, and a 90% H_2O/10% D_2O mixture. The relaxation experiments were performed on samples coming from three different purifications. For the amide exchange experiments, a sample dissolved in H_2O was lyophilized and then dissolved again in 99.996% D_2O (Cambridge Isotope Laboratories). Following the addition of D_2O, ^{15}N HSQC spectra were acquired after 15, 30, 50, and 80 min, 2, 4, 6, 8, 10, and 12 h, and 2, 3, 4, 6, and 12 days.

NMR Spectroscopy. NMR experiments were carried out at 30 °C on either a Varian INOVA 500 (NANUC), 600

(Laval University), or 800 (NANUC) spectrometer, each equipped with a *z*-axis pulsed field gradient and a triple-resonance probe. T_1 experiments were performed using a sensitivity-enhanced inversion−recovery pulse sequence with pulsed field gradients (*22*). Each T_1 spectrum at 500 MHz was acquired with 1024 (t_2) × 80 (t_1) complex data points, spectral widths of 8000 Hz in ^{1}H and 1140 Hz in ^{15}N, and 64 scans per t_1 point. At 600 MHz, T_1 spectra were acquired with 1024 (t_2) × 96 (t_1) complex data points, spectral widths of 10 000 Hz in ^{1}H and 1368 Hz in ^{15}N, and 64 scans. At 800 MHz, spectral widths were 13 523 Hz in ^{1}H and 1824 Hz in ^{15}N with 1514 (t_2) × 128 (t_1) complex data points, and 32 scans were acquired per t_1 increment. The recycle delay was 1.8 s at all fields. T_1 delay times of 11.1 (×2), 22.2, 44.4, 88.8, 177.6, 355.2, 710.4, 1420.8, and 1998 ms were used at 500 MHz, 10.9, 21.8, 43.6, 87.2, 174.4, 348.9, 697.7, 1395.4, and 1995.0 ms at 600 MHz (all acquired in duplicate), and 10.7 (×2), 21.4, 42.7, 85.5, 171.0, 342.0, 684.0, and 1603.2 ms at 800 MHz. T_2 experiments were performed using the BioPack (Varian Inc.) pulse sequence (*23*). Acquisition parameters were identical to those of the T_1 experiments, except that 1024 (t_2) × 128 (t_1) complex data points and 16 scans were collected per t_1 point at 600 MHz, and recycle delays were 2.0, 3.0, and 2.0 s at 500, 600, and 800 MHz, respectively. Delay times of 10, 30, 50, 70, 90, 110, 130, 150, 170, and 190 ms were used at the three fields. {^{1}H}−^{15}N steady-state NOEs were obtained by acquiring spectra with and without ^{1}H saturation applied before the start of the experiments using a pulse sequence obtained from the Kay group (*22*). Spectral widths were identical as for T_1 and T_2. At 500 MHz, 1024 (t_2) × 80 (t_1) complex data points with 104 scans were collected, and 1024 (t_2) × 96 (t_1) complex data points with 128 scans were collected at 600 MHz. A saturation time of 4 s was used in all NOE experiments.

To eliminate the potential effect of sample or field homogeneity degradation over time on measured exponential decays, relaxation delays were acquired in an interleaved manner. For example, the acquisition order for the ^{15}N T_2 experiments was as follows: 10, 50, 90, 130, 170, 30, 70, 110, 150, and 190 ms (*24*, *25*).

Data Analysis. All NMR data were processed with NMRPipe (*26*) and analyzed with NMRView (*27*). The *ranceY.M* macro from the NMRPipe package was used to generate pure absorptive two-dimensional line shapes from the sensitivity-enhanced data. Removal of the residual water signal was performed through the use of time domain polynomial subtraction (NMRPipe function *POLY -time*). ^{1}H−^{15}N spectra were processed using either a 90°- or 60°-shifted sine apodization function in F_2 (^{1}H) and either a 90°- or 60°-shifted sine-squared function in F_1 (^{15}N). The 90° processing was used for the great majority of the residues, but the 60° processing allowed the separation of some peaks exhibiting slight overlapping. Linear prediction was performed in F_1 to extend the time domain by a factor of 1.5; both dimensions were zero filled (NMRPipe function *ZF -auto*) and baseline corrected using the *POLY -auto* function. For each T_1 and T_2 experiment, the spectrum with the shortest relaxation time (highest intensities) was peak picked with NMRView and each ellipse was manually adjusted to fit the peak.

The ^{15}N R_1 and R_2 relaxation rates were determined by fitting T_1 and T_2 curves to a two-parameter function of the form

$$V(t) = V_0 e^{-Rt} \quad (1)$$

where $V(t)$ is the volume after a delay time t, V_0 is the volume at time zero, and R is either $1/T_1$ (R_1) or $1/T_2$ (R_2). Fitting was accomplished using CURVEFIT (A. G. Palmer, Columbia University, New York, NY). R_1 and R_2 uncertainties were calculated using both the Monte Carlo and Jackknife methods; the method giving the highest error was retained, and for each data set, the minimum error used for further calculation was set to the mean error. NOE values were obtained from the ratio of the volumes of experiments recorded with and without proton saturation. The uncertainties on the NOEs were set to 2 times the standard deviation between intensities of duplicate experiments.

^{15}N NMR relaxation was analyzed using contributions from dipole−dipole (DD) and chemical shift anisotropy (CSA) relaxation mechanisms (*28*):

$$R_1 = (d^2/4)[J(\omega_H - \omega_N) + 3J(\omega_N) + 6J(\omega_H + \omega_N)] + c^2 J(\omega_N) \quad (2)$$

$$R_2 = (d^2/8)[4J(0) + J(\omega_H - \omega_N) + 3J(\omega_N) + 6J(\omega_H) + 6J(\omega_H + \omega_N)] + (c^2/6)[4J(0) + 3J(\omega_N)] + R_{ex} \quad (3)$$

$$\mathrm{NOE} = 1 + (d^2/4R_1)(\gamma_N/\gamma_H)[6J(\omega_H + \omega_N) - J(\omega_H - \omega_N)] \quad (4)$$

where $d = \mu_0 h \gamma_N \gamma_H \langle r_{NH}^{-3} \rangle / (8\pi^2)$, $c = \omega_N \Delta\sigma/\sqrt{3}$, μ_0 is the permeability of free space, h is Planck's constant, γ_H and γ_N are the magnetogyric ratios of ^{1}H and ^{15}N, respectively, r_{NH} is the mean nitrogen−hydrogen bond length (taken here to be 1.02 Å), and $\Delta\sigma = \sigma_{||} - \sigma_\perp$ is the CSA, taken here to be −172 ppm. This combination of r_{NH} and CSA typically leads to an average order parameter of 0.85 for rigid secondary structure elements (*29*). $J(\omega)$ denotes the spectral density function; ω_H and ω_N are the Larmor frequencies of ^{1}H and ^{15}N, respectively. The R_{ex} term in eq 3 represents conformational exchange and pseudo-first-order processes occurring on the microsecond-to-millisecond time scale (*30*).

Model-Free Analysis. The amplitudes and time scales of the intramolecular motions of the protein were determined from the relaxation data according to the model-free formalism pioneered by Lipari and Szabo (*31*, *32*) and extended by Clore et al. (*33*, *34*), by using Modelfree (version 4.15, A. G. Palmer, Columbia University) in combination with FastModelfree (*35*). An initial estimate of the overall tumbling (τ_m) of TEM-1 was first obtained from the R_2/R_1 ratio using QUADRIC (A. G. Palmer, Columbia University) using PDB entry 1BTL (*4*). This estimation was made with the 600 MHz data, where three residues with NOE values of <0.65 were not considered as well as 19 residues with high R_2 values ($R_2 \geq \langle R_2 \rangle + \sigma_{R_2}$), unless their corresponding R_1 values were low ($R_1 \leq \langle R_1 \rangle - \sigma_{R_1}$) (*36*). QUADRIC was also used to determine the diffusion tensors for spherical, axially symmetric, and fully anisotropic motional models. The hydrogen atoms were first added to the structure file

using MOLMOL (*37*); the coordinate system of the PDB entry was moved to the center of mass of the molecule using PDBINERTIA (A. G. Palmer, Columbia University), and finally, an estimate of the diffusion tensor was made and the axis of the PDB coordinate system rotated so that they were aligned with the principal axis of the diffusion tensor. The *F* test was used to check the statistical improvement of the fitting to each model.

In this analysis, the spectral density function, $J(\omega)$, chosen to reflect an axially symmetric diffusion tensor, is modeled as (*38*, *39*)

$$J(\omega) = \frac{2}{5} S_f^2 \sum_{j=1}^{3} A_j \left[\frac{S_s^2 \tau_j}{1 + \omega^2 \tau_j^2} + \frac{(1 - S_s^2)\tau_j'}{1 + \omega^2 \tau_j'^2} \right] \quad (5)$$

where $\tau_j' = \tau_j \tau_e/(\tau_j + \tau_e)$, $\tau_1^{-1} = 6D_\perp$, $\tau_2^{-1} = 5D_\perp + D_\parallel$, $\tau_3^{-1} = 2D_\perp + 4D_\parallel$, $D_\perp$ and $D_\parallel$ are the components of an axially symmetric diffusion tensor, $A_1 = (3 \cos^2 \theta - 1)^2/4$, $A_2 = 3 \sin^2 \theta \cos^2 \theta$, and $A_3 = {}^3/_4 \sin^4 \theta$, where θ is the angle between the N−H vector and the unique axis of the principal component of the diffusion tensor. S^2 ($=S_f^2 S_s^2$) is the square of the generalized order parameter characterizing the amplitude of internal motions, and S_f^2 and S_s^2 are the squares of the order parameters for the internal motions on the fast and slow time scales, respectively. τ_e is the effective correlation time for internal motions.

The selection of the dynamics models was carried out using a procedure similar to the one proposed by Mandel et al. (*40*). The five models (derived from eq 5) used to fit our experimental data were

$$\text{model 1: } S^2 \, (\tau_e = 0, R_{ex} = 0, S_f^2 = 1)$$

$$\text{model 2: } S^2, \tau_e \, (R_{ex} = 0, S_f^2 = 1)$$

$$\text{model 3: } S^2, R_{ex} \, (\tau_e = 0, S_f^2 = 1)$$

$$\text{model 4: } S^2, \tau_e, R_{ex} \, (S_f^2 = 1)$$

$$\text{model 5: } S^2, \tau_e, S_f^2 \, (R_{ex} = 0)$$

After manual adjustment of the models, a final optimization of the dynamics parameters was carried out.

Sequence Numbering. Because of technical requirements in the NMR analysis, the sequence numbering used for TEM-1 in this study is different from the one proposed by Ambler (*41*). Although the sequence starts at number 26 to give the active site serine residue the number 70, the numbering is sequential from 26 to 288, so residue numbers 239 and 253 are not skipped.

RESULTS AND DISCUSSION

Backbone Sequential Assignment. The backbone sequential assignment used in this analysis was previously described (*13*). The NMR assignment procedure allowed us to identify the E28G mutation on the third N-terminal residue of the mature protein. As this mutation occurred on the third residue, important changes in the three-dimensional structure were unlikely. However, we recently carried out mutagenesis of the gene to reintroduce Glu28, expressed and purified the ^{15}N-labeled and ^{15}N- and ^{13}C-labeled protein, and carried out the backbone sequential assignment (BMRB accession number 6357). After analysis, we found that for 98.5% of the backbone atoms, chemical shift changes were within the experimental errors (0.02 ppm for ^{1}H, 0.15 ppm for ^{15}N, and 0.20 ppm for ^{13}C), and we concluded that the dynamics of these two proteins would be very similar. Moreover, this E28G mutant was inadvertently used for many years by several groups working on TEM-1 without any change in the enzymatic parameters being noticed, pointing toward the fact that it is very similar to the wild type.

Relaxation Data. We have chosen X-ray structure 1BTL (*4*) of wild-type TEM-1 to fit our experimental NMR relaxation data. From that structure, we can see it is a globular protein of ellipsoidal shape with dimensions of 30 Å × 40 Å × 50 Å. TEM-1 has two domains, a α/β domain made of a five-stranded antiparallel β-sheet (S1−S5) onto which three helices (H1, H10, and H11) are packed toward the solvent interface. The second one, an all-α domain, is made of eight helices (H2−H9) located on the other side of the pleated sheet. There is a large depression at the interface of the two domains, corresponding to the substrate-binding site.

Since TEM-1 gives very widely dispersed two-dimensional ^{15}N HSQC spectra, it was possible to characterize 177 well-resolved peaks at 500 MHz, 198 at 600 MHz, and 227 at 800 MHz, which represent 71, 79, and 91% of the 250 theoretically observable amides, respectively. From these, we have extracted R_1, R_2, and NOE values at 500 and 600 MHz, as well as R_1 and R_2 values at 800 MHz, for a total of 1579 observables to fit in our dynamic analysis. Because spectra were well-resolved, peak volumes based on manually adjusted peak ellipses were used in this analysis, since they can give more accurate results than peak intensities (*42*). Overlapped or very weak resonances were not considered.

R_1 and R_2 values are not sensitive to the same motional frequencies. R_1 values provide information about motional properties with a frequency of approximately 10^8−10^{12} Hz, while R_2 values depend both on motions occurring at these high frequencies and on dynamics on the microsecond-to-millisecond time scale. Via measurement of both R_1 and R_2 relaxation rates, it is therefore possible to obtain dynamic information over a large motional regime (*43*).

Data obtained from the relaxation experiments are of very good quality (Figure 1). The R_1 data exhibit the same pattern at the three fields, and as expected, $R_1^{500} > R_1^{600} > R_1^{800}$. The R_2 values are also in very good agreement at the three fields, and as a result of the CSA contribution to R_2 which is proportional to ω_N^2, $R_2^{800} > R_2^{600} > R_2^{500}$ (*24*). The R_2/R_1 ratio clearly follows the pattern of the R_2, with higher values in some regions such as residues 120−130, 165−175 (Ω-loop), and 210−225, an indication that these residues may undergo conformational exchange phenomena on the microsecond-to-millisecond time scale. It is interesting to note that some disorder was observed for this latter region in high-resolution X-ray structure 1M40 (*5*). NOE values at 500 and 600 MHz also exhibit the same pattern, and they both show atypically high values, even for the N- and C-termini, indicating that TEM-1 is ordered from one extremity to the other. Typically, NOE values near 0.84 (at 600 MHz) indicate a complete lack of higher-frequency backbone motions, while values below 0.84 (at 600 MHz)

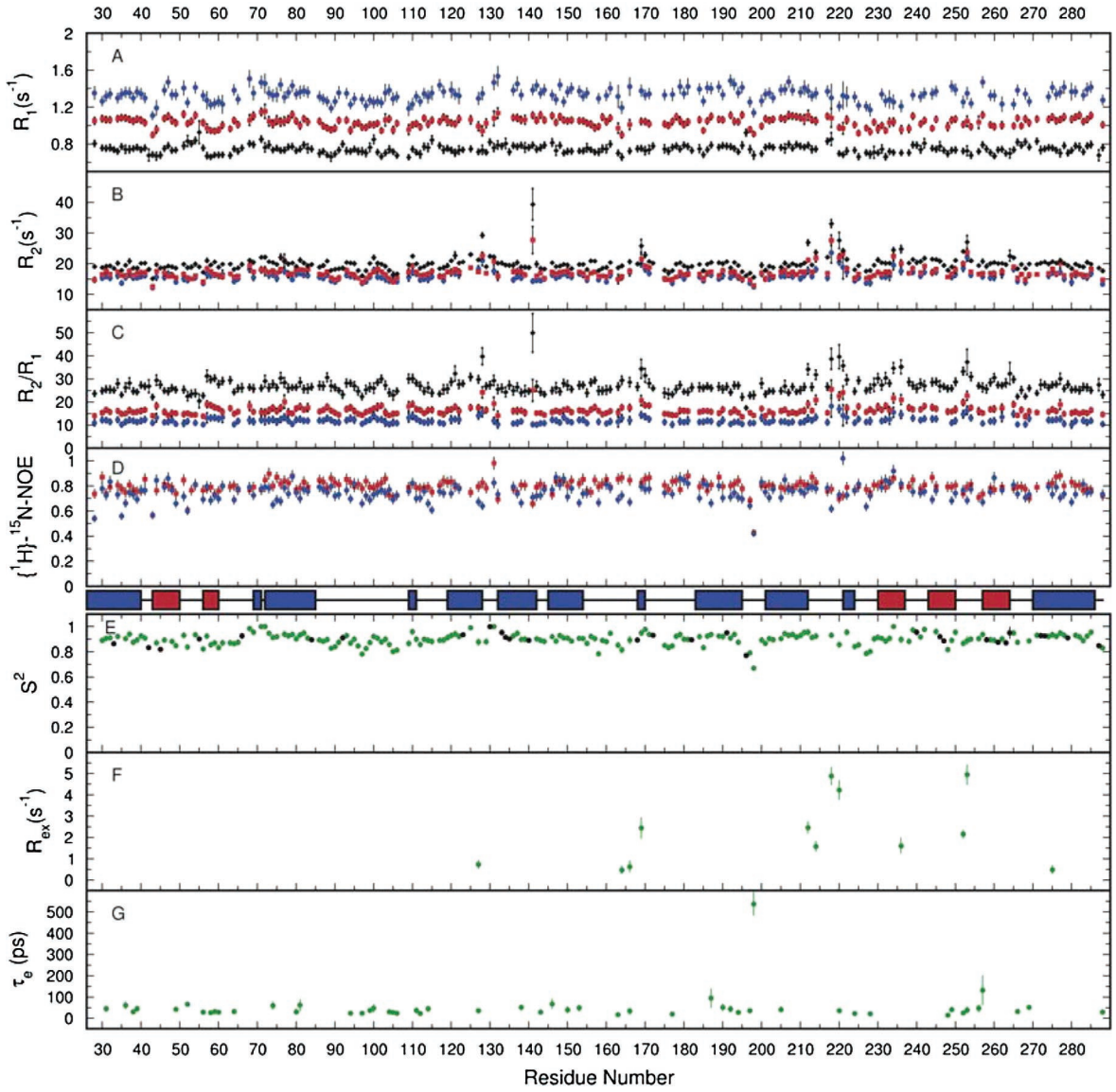

FIGURE 1: Relaxation data for TEM-1: (A) ^{15}N R_1, (B) ^{15}N R_2, (C) R_2/R_1, (D) {^{1}H}−^{15}N NOE at 500 (blue), 600 (red), and 800 MHz (black). Dynamics parameters derived from the model-free analysis of Lipari and Szabo: (E) order parameters (S^2), (F) conformational exchange parameters (R_{ex}), and (G) effective correlation times for internal motions (τ_e). Black dots in the S^2 plot represent data for residues for which data were usable at only 800 MHz. The secondary structure is represented in the middle of the figure; α-helices and β-strands are colored blue and red, respectively.

Table 1: Average Values of Relaxation Parameters Obtained for TEM-1

	500 MHz	600 MHz	800 MHz
R_1 (s^{-1})	1.33 ± 0.07	1.04 ± 0.03	0.745 ± 0.03
R_2 (s^{-1})	15.96 ± 0.83	17.10 ± 0.58	20.05 ± 0.38
R_2/R_1	12.00 ± 1.21	16.52 ± 1.11	27.00 ± 1.69
NOE	0.745 ± 0.04	0.795 ± 0.04	not available

reveal a local flexibility of the protein on the 10^{-12}−10^{-9} s time scale (*44*). The average values for R_1, R_2, and {^{1}H}−^{15}N NOE are listed in Table 1.

Model-Free Analysis. The model-free analysis provides a characterization of both global and local motions. Global tumbling is characterized by the global correlation time (τ_m) as well as parameters describing the anisotropy of the global tumbling. The amplitude of picosecond-to-nanosecond local motions is characterized by an order parameter (S^2) which may take values between 0 and 1, and the time scale of these motions is characterized by a local correlation time τ_e. The typical order parameter observed in the structured regions of well-folded proteins is between 0.80 and 0.90 with an average value of 0.85, and lower for flexible regions.

The model-free analysis presented here is reinforced by the fact that the data were acquired at three different magnetic fields. Such a way to measure ^{15}N relaxation parameters allows sampling of the spectral density function at multiple frequencies and therefore provides a more detailed picture of the distribution of motions associated with the dynamics of a backbone amide N−H bond vector than would be provided from relaxation measurements at just one field (*45*, *46*).

In X-ray structure 1BTL (*4*) of TEM-1, the relative moments of inertia are 1.0, 0.9, and 0.6, indicating the potential significance of motional anisotropy. Moreover, best statistical results from the diffusion tensor analysis were obtained by fitting the data with the axially symmetric model, so we have used this model to fit the global tumbling of TEM-1 and explore its internal backbone dynamics.

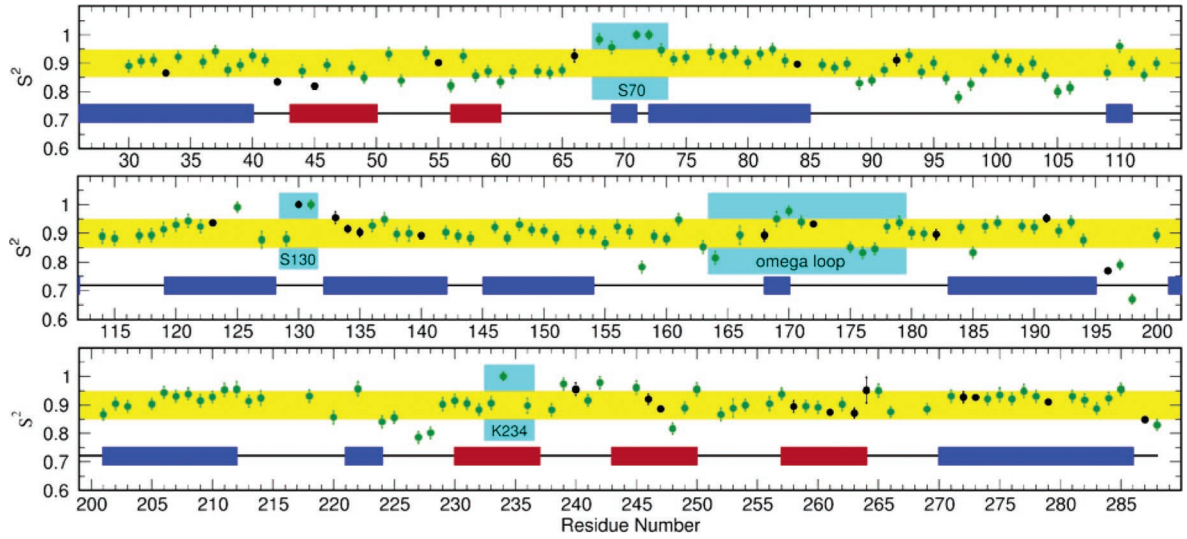

FIGURE 2: Detailed diagram of the S^2 parameters according to the amino acid sequence and the secondary structure elements. α-Helices are colored blue and β-strands red. Black dots represent data for residues for which data were usable at only 800 MHz because of the resolution improvement obtained at this higher field. The yellow stripe, centered on the mean S^2 value, is two standard deviations wide. The Ω-loop is highlighted in cyan, as well as other regions in the proximity of the active site.

Following the model selection, 147 residues (58.8%) were fitted to model 1, indicating that internal motions for these residues are so rapid that their only effect is to reduce the order parameter from 1 to S^2. Forty-two residues (16.8%) were fitted to model 2, which means that for these residues, fast internal motions on the subnanosecond time scale contribute significantly to the observed relaxation. Model 3 was used to fit six residues (Arg164, Leu169, Glu212, Asp214, Gly236, and Arg275) for which a slow (microsecond-to-millisecond) component of motion resulting in exchange broadening was needed. Six residues (Arg94, Ile127, Glu166, Gly218, Leu220, and Asp252) were fitted to model 4, suggesting that for these residues both τ_e and R_{ex} contribute significantly to the relaxation. Finally, four residues (Asp115, His158, Leu198, and Ala227) exhibited a two-time scale contribution to the relaxation, as they were fitted to model 5. Seventeen residues were not well fitted by any model (Gly28, Asp35, Arg43, Ile47, Ser53, Leu76, Thr128, Asn132, Thr141, Thr195, Ala217, Leu221, Gly244, Gly253, Gln267, Ala268, and Ile280). For 29 residues, only R_1 and R_2 values at 800 MHz were available, so only model 1 could be used to fit these residues. Among these, 23 residues fit well with model 1 while six of them could not be fit to any other model due to the lack of information (Gly92, Ser130, Glu168, Gly196, Ile261, and Thr263).

After a final optimization of the dynamics parameters, TEM-1 exhibited a small prolate axial anisotropy with a $D_\parallel/D_\perp$ value of 1.23 ± 0.01 and a global correlation time (τ_m) of 12.41 ± 0.01 ns. The average order parameter (S^2) value obtained for the whole protein is exceptionally high (0.90 ± 0.02) with, in general, higher values for the secondary structure elements and lower values in loops (Figures 2 and 3). The order parameter measures the degree of spatial restriction of the motion; it varies from 0 to 1, in which lower values indicate larger amplitudes of internal motions (*47*). As mentioned in Experimental Procedures, the values of r_{NH} and CSA used here (1.02 Å and −172 ppm, respectively) typically result in a generalized order parameter of 0.85 for the structured regions (α-helices and β-strands), and lower values for exposed loops and termini regions (*29*). Values of 1.02 Å and −160 ppm, respectively, are often found in the literature as they are default values used by many programs. By using these values with our data, we obtained a higher generalized order parameter, with an average value of 0.94. It is interesting to notice that both N- and C-terminal residues exhibit high S^2 values, which is quite unusual among proteins that have been studied to date. Similarly, this clearly indicates a high degree of order for TEM-1 in solution. Few examples of protein backbones showing such a high S^2 (using an r_{NH} of 1.02 Å and a CSA of −172 ppm) are documented. This is the case for ferricytochrome c_{551}, a small 8.7 kDa metalloprotein from *Pseudomonas aeruginosa* (*48*), for which an average S^2 of 0.92 ± 005 was measured using similar values of r_{NH} and CSA as we have used (1.02 Å and −173 ppm, respectively).

Active Site. An interesting point emerging from our data is the rigidity of the backbone of many important residues in the active site of TEM-1. As shown in Figure 3, several highly ordered residues (S^2 > 0.94) are within 4 Å of Ser70, including Met69, Phe72, Lys73, Asn170, the Ser130-Asp131-Asn132 motif (also called the SDN loop, a universally conserved motif in class A enzymes), Lys234, and potentially other residues for which data were unavailable. These residues are shielding Ser70, but there is still a well-exposed region allowing direct access to this residue. These results indicate that the active site is very well ordered on the picosecond-to-nanosecond time scale, even for the free form of the enzyme. This high degree of order could indicate that residues implicated in catalysis are properly positioned to play their role as soon as a target enters the active site.

In agreement with our results are those of the MD study of Suarez et al., who have reported a root-mean-square deviation (rmsd) for the heavy atoms of only 1.3 Å between the simulated free form of TEM-1 and the X-ray structure, indicating that there were only slight structural changes occurring on the time scale that was studied. These changes were located in loops and in solvent-exposed α-helices. Following the simulation they did with the substrate, they concluded that there was a diminution of the flexibility of

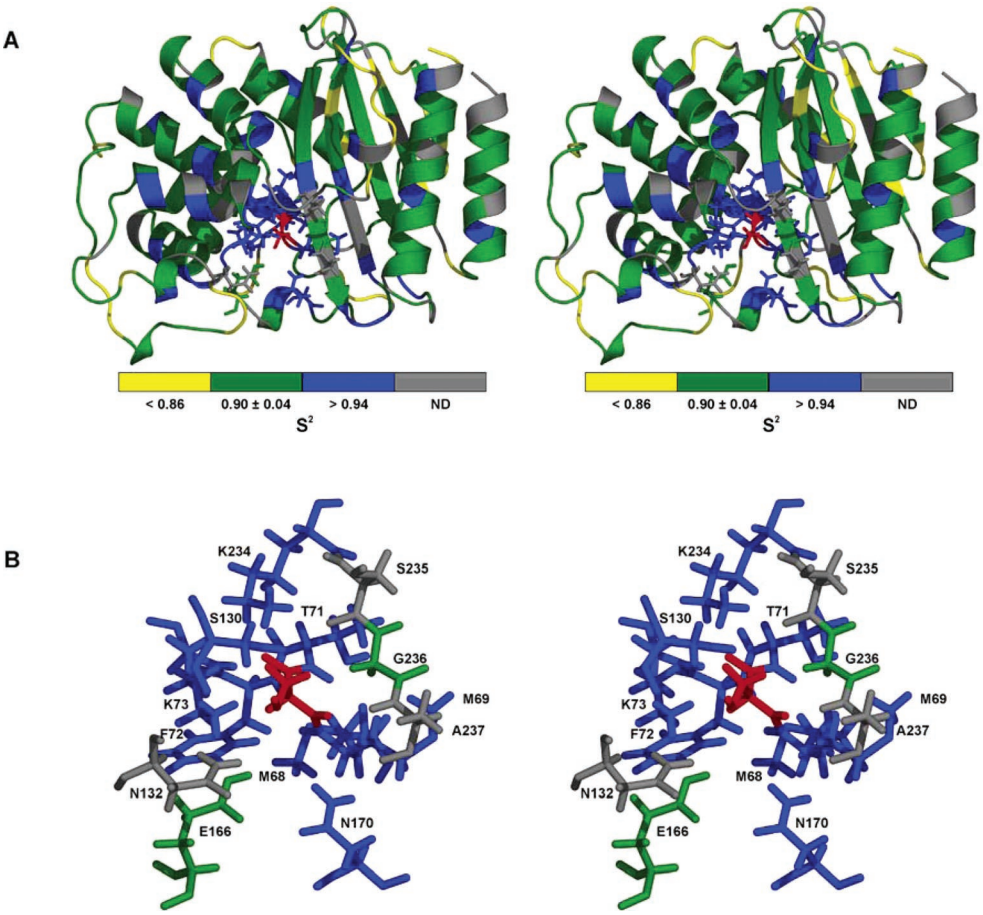

FIGURE 3: (A) Stereoview of the mapping of backbone S^2 values on the structure of TEM-1. The catalytic serine is colored red, and all the residues within a 4 Å radius are shown as sticks. (B) Expansion of the region surrounding Ser70 (red) shown in stereo. Side chain atoms are colored according to the backbone S^2 value. This figure and all other molecular representations of TEM-1 in this paper were made with PyMOL (*56*) using PDB entry 1BTL.

TEM-1 upon binding, indicating an even more rigid protein in the ligand-bound form.

Lower values of S^2 are principally found in four loops of the protein, concerning the regions of residues 95−98, 102−108, 196−200, and 224−230. All of these loops are solvent-exposed. Tyr105, located in one of these flexible loops, was recently proposed to be greatly important for substrate stabilization and discrimination in TEM-1 (*49*), a function that correlates well with the flexibility observed here.

Ω-*Loop*. The Ω-loop, bearing Glu166, is a unique feature of class A β-lactamases, and it is therefore the source of many investigations. From their 1.2 ns MD simulation, Suarez et al. (*6*) have concluded that the Ω-loop in solution only slightly deviated from the crystal structure and that its flexibility was similar to that of the entire protein. Those results are not in agreement with the study of Vijayakumar et al. (*18*), who have predicted mobility for this loop to allow the Glu166 to act as the catalytic base in acylation. A flaplike motion of the Ω-loop was also observed in a recent 5 ns MD simulation (*9*). This flaplike motion of the Ω-loop involves the largest motions observed in this simulation, with a rmsd of up to 4.5 Å for a portion of the Ω-loop. Motion of this magnitude at the time scale probed in a 5 ns MD simulation should lead to order parameters that are well below 0.8. However, from our NMR relaxation data, the Ω-loop exhibited an average S^2 of 0.90 ± 0.02, similar to that obtained for the rest of the protein. This is a high degree of order for an exposed loop, and it clearly indicates that the magnitude of movements in this loop is very small, at least on the picosecond-to-nanosecond time scale, which is the same time scale probed by MD studies.

Chemical Exchange. On the other hand, to fit the data to a suitable model, 12 residues needed the exchange term (R_{ex}) which accounts for exchange phenomena on the microsecond-to-millisecond time scale (I127, R164, E166, L169, E212, D214, G218, L220, G236, D252, L254, and R275). These residues are plotted in Figure 1F and mapped onto the protein structure in Figure 4. The necessity of adding this term means that for these residues, additional relaxation effects due to slow motions can contribute to the transverse relaxation rate (R_2). Dynamical processes in that range are similar in time scale to many biochemical events, and therefore, characterization of R_{ex} in biomolecules provides a tremendous opportunity for elucidation of functional dynamics (*50*). The majority of these residues (eight) are located in loops; four are in helices, and only one is in a β-strand. In the Ω-loop, three residues required an R_{ex} term (R164, E166, and L169); this could be due to loop movements on the microsecond-to-millisecond time scale. It could also be due to the Pro167 residue which could experience cis−trans isomerization on this time scale. This residue was shown to be in the cis conformation in all X-ray structures to properly orient the Glu166 toward the active site (e.g., 1BTL, 1ERM, and 1ERQ). Four residues were unusable in our analysis because

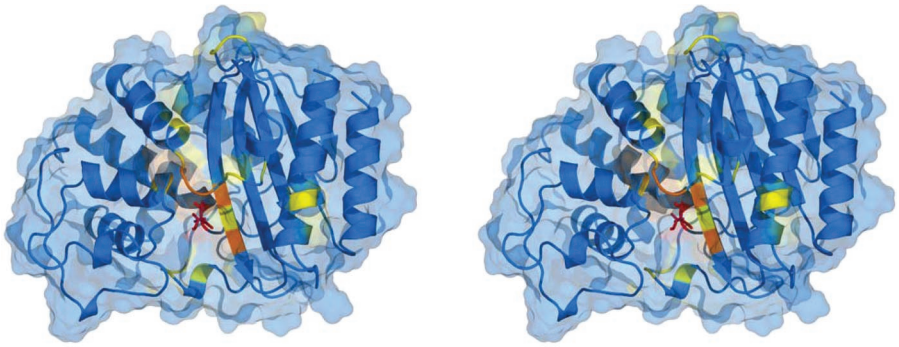

FIGURE 4: Stereoview of TEM-1 where residues that required a R_{ex} term for fitting the data in the model-free analysis are colored yellow. Residues which were unusable because of their weak resonances are colored orange (K215, V216, S235, and A237), and the catalytic serine is shown as sticks (red).

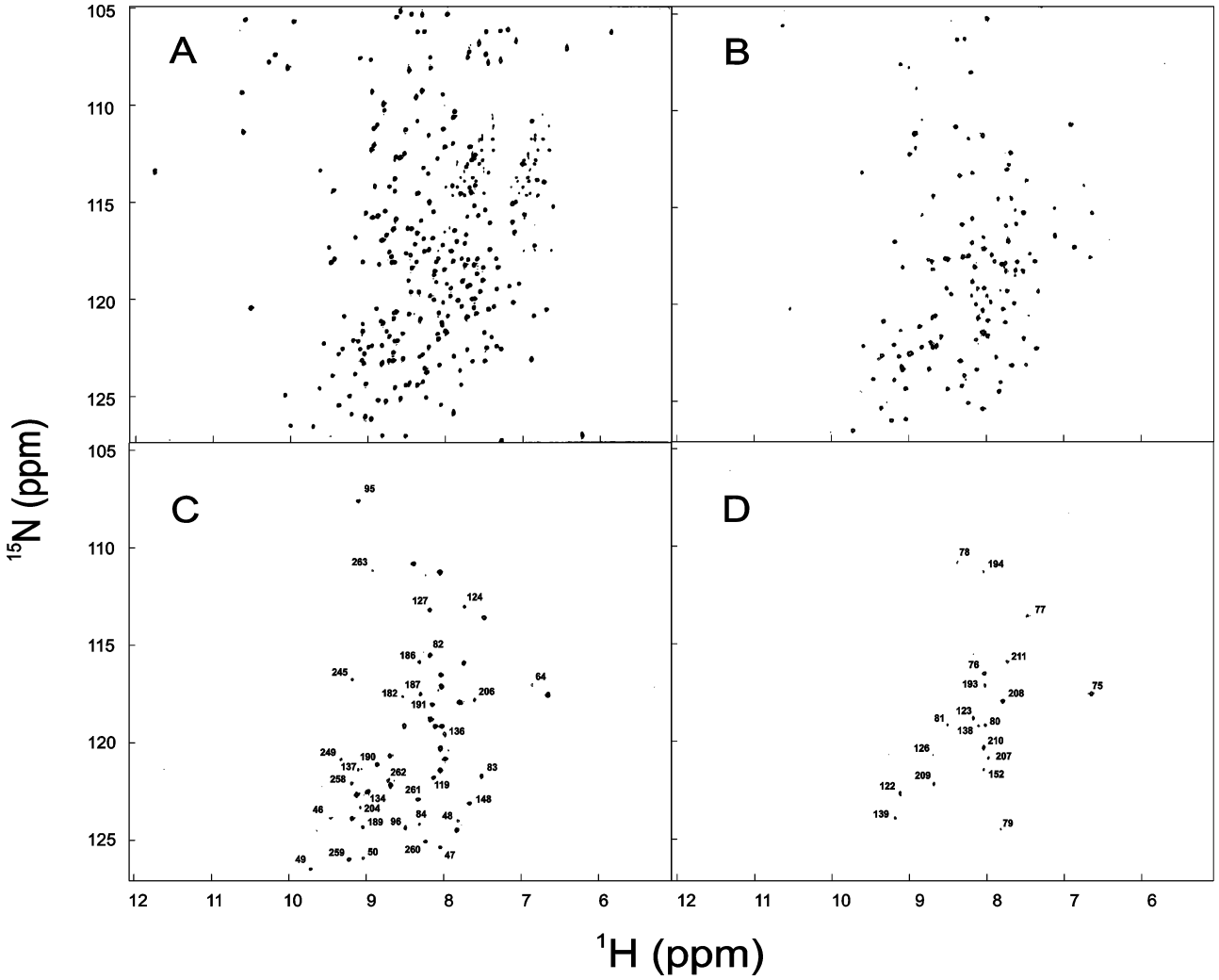

FIGURE 5: ^{15}N HSQC spectra of TEM-1 before (A) or 15 min (B), 2 days (C), or 12 days (D) after addition of D_2O at 30 °C. Peaks of the last two spectra (C and D) are labeled according to residue number. Only peaks that were absent in spectrum D are labeled in spectrum C.

of their weak resonances, a consequence of potential exchange broadening; these are Lys215, Val216, Ser235, and Ala237. By looking at the three-dimensional structure, we can see that Lys215 and Val216 are located in the solvent-exposed, second hinge region (212−222) connecting the two domains of the protein, and they are directly facing Ser235 and Ala237, located in the S3 strand on either side of Gly236, which exhibits conformational exchange (see Figure 4). All these residues are known to be catalytically relevant, and this exchange broadening of their resonances could reflect important ligand-binding-related motions in the active site on the microsecond-to-millisecond time scale.

Internal Correlation Time. The internal correlation time, τ_e, although rarely obtained with >20% uncertainty, likewise affords some estimate of the time scale of bond vector motion (*50*). From TEM-1 dynamics, we have obtained an average value for τ_e of 35.9 ± 13.5 ps.

Amide Exchange Experiments. Labile hydrogens on proteins are continually exchanging with hydrogens from solvent at different rates depending on various aspects of their

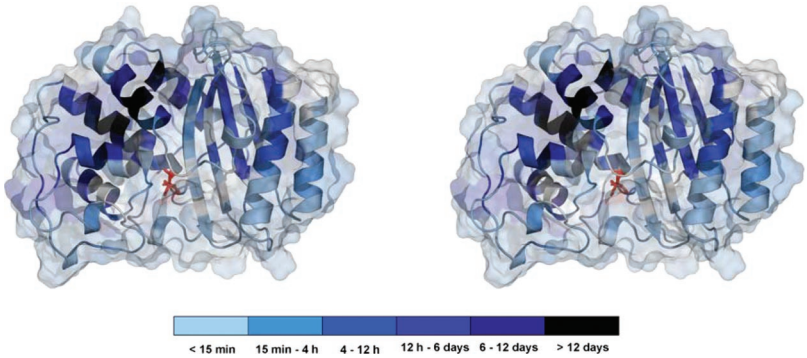

FIGURE 6: Stereo mapping of the amide exchange rate. The catalytic serine is colored red.

environment, such as their exposure to the solvent or their involvement in H-bonds. Amide exchange experiments allow the determination of the degree of exposure of amide protons to the solvent on a time scale of minutes to days. As some amides are completely buried in the core of proteins and are not exposed to the solvent, their eventual exposure implies concerted motions of numerous groups of atoms in the protein. It was proposed that this kind of "breathing" occurs via "unfolding equilibria" that prevail even at temperatures far below the denaturation transition of the native protein (*51*, *52*). Figure 5 shows HSQC spectra acquired at various times after the beginning of the experiment. Fifteen minutes following the dissolution in D_2O, the amides of 108 residues (43%) were already exchanged and were therefore not visible in the HSQC spectrum. These fast-exchange-rate residues are mainly located in exposed loops. Sixty-six residues have exchanged between 15 min and 2 days and 34 between 2 and 12 days; we characterized them as intermediate- and slow-exchange-rate residues, respectively. After 12 days at 30 °C, there were still 18 residues that had not exchanged (Leu75, Leu76, Cys77, Gly78, Ala79, Val80, Leu81, Leu122, Cys123, Leu138, Leu139, Leu193, Leu194, Leu207, Ile208, Asp209, Trp210, and Met211). All of these are in the same region of the protein, and surprisingly, they are all located in α-helices rather than in β-sheets (Figure 6). Thirteen of these residues are hydrophobic (nine are leucines), and they constitute a very important hydrophobic cluster in the protein, with an accessible surface area (ASA) around zero, as calculated using VADAR (*53*). In the center of this cluster are located the two cysteines involved in the sole disulfide bridge of TEM-1 locking together helices H3 and H5. Unfolding−refolding experiments carried out via CD and fluorescence (*54*) have shown that removal of this disulfide bridge dramatically increases the sensitivity to thermal inactivation. Our data suggest that it is very likely that this region would be the last to unfold during the denaturation process.

Dynamic Studies of TEM-1 in Association with a Substrate or an Inhibitor. NMR characterization of the dynamics data of TEM-1 in association with a relevant substrate or inhibitor would have been of great interest in our study, but it is technically impossible to carry out due to the intrinsic properties of this enzyme which hydrolyzes substrates too quickly for NMR experiments to be carried out. Today, in silico methods (e.g., MD and QM/MM) are the most appropriate for studying such complexes, and our experimental data represent a valuable tool that will be used to validate, improve, or develop simulations to better characterize the dynamics of TEM-1, and potentially of other similar enzymes. However, on the basis of the unusually high level of order observed in the apo form, and previous studies of TEM-1 comparing X-ray thermal factors and the Gaussian Network Model (*55*), we do not expect that the binding of a substrate will lead to an increase in the overall level of order of the enzyme. Consequently, it is unlikely that unfavorable changes in conformational entropy would contribute to binding affinity. If there are changes in the fast dynamics upon binding, it could, however, be that binding actually induces a favorable loss of order in TEM-1. It will therefore be very insightful to obtain simulations of TEM-1 in the apo form that are in agreement with our experimental data and to subsequently simulate various complexes of TEM-1.

CONCLUSION

This study reports the first experimental characterization of site-specific dynamics of a class A β-lactamase. Our results revealed that the backbone of TEM-1 in the free form is unusually rigid across the entire sequence. Although previous data did not suggest that TEM-1 would be a flexible protein, there were no indications that TEM-1 would be one of the most rigid proteins characterized to date, with order parameters of 0.90 ± 0.02 across the entire sequence compared to the typical order parameters of 0.85 observed in secondary structure elements of most proteins. We have shown that many important residues in the vicinity of the active site have S^2 values of >0.94, indicating very limited motions on the picosecond-to-nanosecond time scale for the backbone of these residues. This suggests that an unfavorable loss in conformational entropy may not be associated with substrate binding. We have also observed evidence of the presence of microsecond-to-millisecond motions for important residues located in the active site and in the Ω-loop. Motions on this time scale can affect enzyme catalysis, rate-limiting conformational transitions, and ligand−protein recognition. It would therefore be of interest to study changes in the dynamics of TEM-1 mutants which are catalytically impaired.

For the most part, our results are in good agreement with simulations, showing that these two different techniques can interact positively to answer a common dynamical question in the same time scale. Moreover, our experimental results will be extremely valuable in validating and/or developing better simulations to improve these techniques for the study of β-lactamases and β-lactamase complexes. Finally, it will be interesting to study other class A β-lactamases, allowing

us to determine if very high rigidity is a general feature of this family of enzymes.

ACKNOWLEDGMENT

We thank Leigh Willard for the maintenance of the computing infrastructure and Dr. Arthur G. Palmer for providing Modelfree. We are also grateful to Drs. Marvin W. Makinen and Roger C. Levesque for providing help at the beginning of this project and to Olivier Julien, Katia Lecours, and Sabrina Simard for technical help. We thank the Canadian NMR Center (NANUC) for the NMR time at 500 and 800 MHz.

SUPPORTING INFORMATION AVAILABLE

R_1 (S1 and S2), R_2 (S3 and S4), and $^{15}N-\{^1H\}$ NOE data (S5 and S6) measured at 500, 600, and 800 MHz and model-free analysis of relaxation data (S7−S10). This material is available free of charge via the Internet at http://pubs.acs.org.

REFERENCES

1. Walsh, C. (2000) Molecular mechanisms that confer antibacterial drug resistance, *Nature 406*, 775−81.
2. Ambler, R. P. (1980) The structure of β-lactamases, *Philos. Trans. R. Soc. London, Ser. B 289*, 321−31.
3. Strynadka, N. C., Adachi, H., Jensen, S. E., Johns, K., Sielecki, A., Betzel, C., Sutoh, K., and James, M. N. (1992) Molecular structure of the acyl-enzyme intermediate in β-lactam hydrolysis at 1.7 Å resolution, *Nature 359*, 700−5.
4. Jelsch, C., Mourey, L., Masson, J. M., and Samama, J. P. (1993) Crystal structure of *Escherichia coli* TEM1 β-lactamase at 1.8 Å resolution, *Proteins 16*, 364−83.
5. Minasov, G., Wang, X., and Shoichet, B. K. (2002) An ultrahigh-resolution structure of TEM-1 β-lactamase suggests a role for Glu166 as the general base in acylation, *J. Am. Chem. Soc. 124*, 5333−40.
6. Diaz, N., Sordo, T. L., Merz, K. M., Jr., and Suarez, D. (2003) Insights into the acylation mechanism of class A β-lactamases from molecular dynamics simulations of the TEM-1 enzyme complexed with benzylpenicillin, *J. Am. Chem. Soc. 125*, 672−84.
7. Meroueh, S. O., Fisher, J. F., Schlegel, H. B., and Mobashery, S. (2005) Ab initio QM/MM study of class A β-lactamase acylation: Dual participation of Glu166 and Lys73 in a concerted base promotion of Ser70, *J. Am. Chem. Soc. 127*, 15397−407.
8. Oliva, M., Dideberg, O., and Field, M. J. (2003) Understanding the acylation mechanisms of active-site serine penicillin-recognizing proteins: A molecular dynamics simulation study, *Proteins 53*, 88−100.
9. Roccatano, D., Sbardella, G., Aschi, M., Amicosante, G., Bossa, C., Nola, A. D., and Mazza, F. (2005) Dynamical Aspects of TEM-1 β-Lactamase Probed by Molecular Dynamics, *J. Comput.-Aided Mol. Des. 19*, 329−40.
10. Mustafi, D., Hofer, J. E., Huang, W., Palzkill, T., and Makinen, M. W. (2004) Chromophoric spin-labeled β-lactam antibiotics for ENDOR structural characterization of reaction intermediates of class A and class C β-lactamases, *Spectrochim. Acta, Part A 60*, 1279−89.
11. Mustafi, D., Sosa-Peinado, A., Gupta, V., Gordon, D. J., and Makinen, M. W. (2002) Structure of spin-labeled methylmethanethiolsulfonate in solution and bound to TEM-1 β-lactamase determined by electron nuclear double resonance spectroscopy, *Biochemistry 41*, 797−808.
12. Damblon, C., Raquet, X., Lian, L. Y., Lamotte-Brasseur, J., Fonze, E., Charlier, P., Roberts, G. C., and Frere, J. M. (1996) The catalytic mechanism of β-lactamases: NMR titration of an active-site lysine residue of the TEM-1 enzyme, *Proc. Natl. Acad. Sci. U.S.A. 93*, 1747−52.
13. Savard, P. Y., Sosa-Peinado, A., Levesque, R. C., Makinen, M. W., and Gagne, S. M. (2004) ^1H, ^{13}C and ^{15}N backbone resonance assignments for TEM-1, a 28.9 kDa β-lactamase from *E. coli*, *J. Biomol. NMR 29*, 433−4.
14. Golemi-Kotra, D., Meroueh, S. O., Kim, C., Vakulenko, S. B., Bulychev, A., Stemmler, A. J., Stemmler, T. L., and Mobashery, S. (2004) The importance of a critical protonation state and the fate of the catalytic steps in class A β-lactamases and penicillin-binding proteins, *J. Biol. Chem. 279*, 34665−73.
15. Maveyraud, L., Massova, I., Birck, C., Kazuyuki, M., Samama, J. P., and Mobashery, S. (1996) Cristal Structure of 6α-(Hydroxymethyl)penicillanate Complexed to the TEM-1 β-lactamase from *Escherichia coli*: Evidence on the Mechanism of Action of a Novel Inhibitor Designed by a Computer-Aided Process, *J. Am. Chem. Soc. 118*, 7435−40.
16. Herzberg, O., and Moult, J. (1987) Bacterial resistance to β-lactam antibiotics: Crystal structure of β-lactamase from *Staphylococcus aureus* PC1 at 2.5 Å resolution, *Science 236*, 694−701.
17. Lamotte-Brasseur, J., Dive, G., Dideberg, O., Charlier, P., Frere, J. M., and Ghuysen, J. M. (1991) Mechanism of acyl transfer by the class A serine β-lactamase of *Streptomyces albus* G, *Biochem. J. 279* (Part 1), 213−21.
18. Vijayakumar, S., Ravishanker, G., Pratt, R. F., and Beveridge, D. L. (1995) Molecular Dynamics Simulation of a Class A β-Lactamase: Structural and Mechanistic Implications, *J. Am. Chem. Soc. 117*, 1722−30.
19. Swaren, P., Maveyraud, L., Guillet, V., Masson, J. M., Mourey, L., and Samama, J. P. (1995) Electrostatic analysis of TEM1 β-lactamase: Effect of substrate binding, steep potential gradients and consequences of site-directed mutations, *Structure 3*, 603−13.
20. Fisher, J. F., Meroueh, S. O., and Mobashery, S. (2005) Bacterial resistance to β-lactam antibiotics: Compelling opportunism, compelling opportunity, *Chem. Rev. 105*, 395−424.
21. Sosa-Peinado, A., Mustafi, D., and Makinen, M. W. (2000) Overexpression and biosynthetic deuterium enrichment of TEM-1 β-lactamase for structural characterization by magnetic resonance methods, *Protein Expression Purif. 19*, 235−45.
22. Farrow, N. A., Muhandiram, R., Singer, A. U., Pascal, S. M., Kay, C. M., Gish, G., Shoelson, S. E., Pawson, T., Forman-Kay, J. D., and Kay, L. E. (1994) Backbone dynamics of a free and phosphopeptide-complexed Src homology 2 domain studied by ^{15}N NMR relaxation, *Biochemistry 33*, 5984−6003.
23. Zhu, G., Xia, Y., Nicholson, L. K., and Sze, K. H. (2000) Protein dynamics measurements by TROSY-based NMR experiments, *J. Magn. Reson. 143*, 423−6.
24. Gagne, S. M., Tsuda, S., Spyracopoulos, L., Kay, L. E., and Sykes, B. D. (1998) Backbone and methyl dynamics of the regulatory domain of troponin C: Anisotropic rotational diffusion and contribution of conformational entropy to calcium affinity, *J. Mol. Biol. 278*, 667−86.
25. Tjandra, N., Wingfield, P., Stahl, S., and Bax, A. (1996) Anisotropic rotational diffusion of perdeuterated HIV protease from ^{15}N NMR relaxation measurements at two magnetic fields, *J. Biomol. NMR 8*, 273−84.
26. Delaglio, F., Grzesiek, S., Vuister, G. W., Zhu, G., Pfeifer, J., and Bax, A. (1995) NMRPipe: A multidimensional spectral processing system based on UNIX pipes, *J. Biomol. NMR 6*, 277−93.
27. Johnson, B. A., and Blevins, R. A. (1994) NMRView: A computer program for the visualization and analysis of NMR data, *J. Biomol. NMR 4*, 603−14.
28. Abragam, A. (1961) *Principles of nuclear magnetism*, Clarendon Press, Oxford, U.K.
29. Palmer, A. G., III (2001) NMR probes of molecular dynamics: Overview and comparison with other techniques, *Annu. Rev. Biophys. Biomol. Struct. 30*, 129−55.
30. Bloom, M., Reeves, L. W., and Wells, E. J. (1965) Spin−Echoes and Chemical Exchange, *J. Chem. Phys. 42*, 1615.
31. Lipari, G., and Szabo, A. (1982) Model-Free Approach to the Interpretation of Nuclear Magnetic Resonance Relaxation in Macromolecules. 1. Theory and Range of Validity, *J. Am. Chem. Soc. 104*, 4546−59.
32. Lipari, G., and Szabo, A. (1982) Model-Free Approach to the Interpretation of Nuclear Magnetic Resonance Relaxation in Macromolecules. 2. Analysis of Experimental Results, *J. Am. Chem. Soc. 104*, 4559−70.
33. Clore, G. M., Driscoll, P. C., Wingfield, P. T., and Gronenborn, A. M. (1990) Analysis of the backbone dynamics of interleukin-1β using two-dimensional inverse detected heteronuclear ^{15}N-^1H NMR spectroscopy, *Biochemistry 29*, 7387−401.
34. Clore, G. M., Szabo, A., Bax, A., Kay, L. E., Driscoll, P. C., and Gronenborn, A. M. (1990) Deviations from the Simple Two-

Parameter Model-Free Approach to the Interpretation of Nitrogen-15 Nuclear Magnetic Relaxation of Proteins, *J. Am. Chem. Soc. 112*, 4989−91.
35. Cole, R., and Loria, J. P. (2003) FAST-Modelfree: A program for rapid automated analysis of solution NMR spin-relaxation data, *J. Biomol. NMR 26*, 203−13.
36. Pawley, N. H., Wang, C., Koide, S., and Nicholson, L. K. (2001) An improved method for distinguishing between anisotropic tumbling and chemical exchange in analysis of ^{15}N relaxation parameters, *J. Biomol. NMR 20*, 149−65.
37. Koradi, R., Billeter, M., and Wuthrich, K. (1996) MOLMOL: A program for display and analysis of macromolecular structures, *J. Mol. Graphics 14*, 51−5, 29−32.
38. Woessner, D. E. (1962) Nuclear Spin Relaxation in Ellipsoids Undergoing Rotational Brownian Motion, *J. Chem. Phys. 37*, 647−54.
39. Barbato, G., Ikura, M., Kay, L. E., Pastor, R. W., and Bax, A. (1992) Backbone dynamics of calmodulin studied by ^{15}N relaxation using inverse detected two-dimensional NMR spectroscopy: The central helix is flexible, *Biochemistry 31*, 5269−78.
40. Mandel, A. M., Akke, M., and Palmer, A. G., III (1995) Backbone dynamics of *Escherichia coli* ribonuclease HI: Correlations with structure and function in an active enzyme, *J. Mol. Biol. 246*, 144−63.
41. Ambler, R. P., Coulson, A. F., Frere, J. M., Ghuysen, J. M., Joris, B., Forsman, M., Levesque, R. C., Tiraby, G., and Waley, S. G. (1991) A standard numbering scheme for the class A β-lactamases, *Biochem. J. 276* (Part 1), 269−70.
42. Viles, J. H., Duggan, B. M., Zaborowski, E., Schwarzinger, S., Huntley, J. J., Kroon, G. J., Dyson, H. J., and Wright, P. E. (2001) Potential bias in NMR relaxation data introduced by peak intensity analysis and curve fitting methods, *J. Biomol. NMR 21*, 1−9.
43. Kay, L. E., Torchia, D. A., and Bax, A. (1989) Backbone dynamics of proteins as studied by ^{15}N inverse detected heteronuclear NMR spectroscopy: Application to staphylococcal nuclease, *Biochemistry 28*, 8972−9.
44. Cordier, F., Caffrey, M., Brutscher, B., Cusanovich, M. A., Marion, D., and Blackledge, M. (1998) Solution structure, rotational diffusion anisotropy and local backbone dynamics of *Rhodobacter capsulatus* cytochrome c_2, *J. Mol. Biol. 281*, 341−61.
45. Andrec, M., Montelione, G. T., and Levy, R. M. (1999) Estimation of dynamic parameters from NMR relaxation data using the Lipari-Szabo model-free approach and Bayesian statistical methods, *J. Magn. Reson. 139*, 408−21.
46. Campbell, A. P., Spyracopoulos, L., Irvin, R. T., and Sykes, B. D. (2000) Backbone dynamics of a bacterially expressed peptide from the receptor binding domain of *Pseudomonas aeruginosa* pilin strain PAK from heteronuclear ^{1}H-^{15}N NMR spectroscopy, *J. Biomol. NMR 17*, 239−55.
47. Cavanagh, J., Fairbrother, W. J., Palmer, A. G., III, and Slelton, N. J. (1996) *Protein NMR Spectroscopy: Principles and Practice*, Academic Press, San Diego.
48. Russell, B. S., Zhong, L., Bigotti, M. G., Cutruzzola, F., and Bren, K. L. (2003) Backbone dynamics and hydrogen exchange of *Pseudomonas aeruginosa* ferricytochrome c_{551}, *J. Biol. Inorg. Chem. 8*, 156−66.
49. Doucet, N., De Wals, P. Y., and Pelletier, J. N. (2004) Site-saturation mutagenesis of Tyr-105 reveals its importance in substrate stabilization and discrimination in TEM-1 β-lactamase, *J. Biol. Chem. 279*, 46295−303.
50. Kempf, J. G., and Loria, J. P. (2003) Protein dynamics from solution NMR: Theory and applications, *Cell. Biochem. Biophys. 37*, 187−211.
51. Wuthrich, K. (1981) Nuclear magnetic resonance studies of internal mobility in globular proteins, *Biochem. Soc. Symp*., 17−37.
52. Hvidt, A., and Nielsen, S. O. (1966) Hydrogen exchange in proteins, *Adv. Protein Chem. 21*, 287−386.
53. Willard, L., Ranjan, A., Zhang, H., Monzavi, H., Boyko, R. F., Sykes, B. D., and Wishart, D. S. (2003) VADAR: A web server for quantitative evaluation of protein structure quality, *Nucleic Acids Res. 31*, 3316−9.
54. Vanhove, M., Guillaume, G., Ledent, P., Richards, J. H., Pain, R. H., and Frere, J. M. (1997) Kinetic and thermodynamic consequences of the removal of the Cys-77-Cys-123 disulphide bond for the folding of TEM-1 β-lactamase, *Biochem. J. 321* (Part 2), 413−7.
55. Yang, L. W., and Bahar, I. (2005) Coupling between catalytic site and collective dynamics: A requirement for mechanochemical activity of enzymes, *Structure 13*, 893−904.
56. DeLano, W. L. (2002) *PyMol*, DeLano Scientific, San Carlos, CA.

BI060414Q